1-1-2009

Coulomb-Field-Induced Conversion of a High-Energy Photon into a Pair Assisted by a Counterpropagating Laser Beam

Erik Lotstedt

Ulrich D. Jentschura
Missouri University of Science and Technology, ulj@mst.edu

Christoph H. Keitel

Recommended Citation

E. Lotstedt et al., "Coulomb-Field-Induced Conversion of a High-Energy Photon into a Pair Assisted by a Counterpropagating Laser Beam," *New Journal of Physics*, vol. 11, IOP Publishing, Jan 2009.
The definitive version is available at https://doi.org/10.1088/1367-2630/11/1/013054

New Journal of Physics
The open-access journal for physics

Coulomb-field-induced conversion of a high-energy photon into a pair assisted by a counterpropagating laser beam

Erik Lötstedt[1], **Ulrich D Jentschura and Christoph H Keitel**
Max-Planck-Institut für Kernphysik, Postfach 103980,
69029 Heidelberg, Germany
E-mail: Erik.Loetstedt@mpi-hd.mpg.de, Jentschura@mpi-hd.mpg.de and Keitel@mpi-hd.mpg.de

New Journal of Physics **11** (2009) 013054 (17pp)
Received 7 November 2008
Published 30 January 2009
Online at http://www.njp.org/
doi:10.1088/1367-2630/11/1/013054

Abstract. The laser-induced modification of a fundamental process of quantum electrodynamics, the conversion of a high-energy gamma photon in the Coulomb field of a nucleus into an electron–positron pair, is studied theoretically. Although the employed formalism allows for the general case where the gamma photon and laser photons cross at an arbitrary angle, we here focus on a theoretically interesting and numerically challenging setup, where the laser beam and gamma photon counterpropagate and impinge on a nucleus at rest. For a peak laser field smaller than the critical Schwinger field and gamma photon energy larger than the field-free threshold, the total cross section is verified to be almost unchanged with respect to the field-free case, whereas the differential cross section is drastically modified by the laser field. The modification of the differential cross section is explained by classical arguments. We also find the laser-dependent maximal energy of the produced pair and point out several interesting features of the angular spectrum.

[1] Author to whom any correspondence should be addressed.

Contents

1. Introduction

The creation of an electron–positron pair by an external electromagnetic field is a striking manifestation of the equivalence of matter and energy. That not only energetic photon fields, but also strong, macroscopic electric fields can produce pairs was first predicted by Sauter [1] and later considered by Schwinger [2]. The basic prediction is that pairs are spontaneously created, but the rate is exponentially damped unless the electric field strength exceeds the so-called critical field $E_c = m^2/|e|$, where m is the electron mass, $e = -|e|$ the electron charge, and we use natural units such that $c = \hbar = 1$. The transition from the nonperturbative, tunnelling regime for pair production to high-frequency perturbative pair production was studied in [3]–[5]. At present, the strongest electromagnetic fields available in the laboratory are laser fields. However, a plane laser wave cannot alone produce any pairs from the vacuum due to the impossibility of satisfying energy–momentum conservation. Just like in a static magnetic field [6, 7], a probing particle is needed in order to obtain a nonvanishing pair production rate. If the laser wave is not plane but a focused pulse [8], or a standing laser wave [9]–[11], pair production is possible without a second agent.

Laser-induced pair production with an additional source of momentum was first investigated theoretically in the context of pair production by simultaneous absorption of one nonlaser-mode photon and a number of laser-mode photons [12, 13]; quite recently, this process was also observed experimentally [14, 15]. Another possibility discussed in the literature is laser-induced pair creation in the vicinity of a nucleus. Unfortunately, for a nucleus at rest, the pair production rates are very low [16]–[20]. Recently, this process has been re-examined, with the idea of introducing a moving nucleus [21]–[27]. By letting the nucleus collide head-on with the laser beam at high Lorentz factor γ, in the rest frame of the nucleus the frequency of the laser beam will be blue-shifted or enhanced with a factor of approximately 2γ. In this way, the peak electric field seen by the nucleus in its rest frame approaches the critical field, and the rates are calculated to reach observable values. Other promising schemes are [28]–[30], where muon–antimuon pairs are created from a laser-driven positronium atom, and [31], where the photon-assisted Schwinger effect is considered.

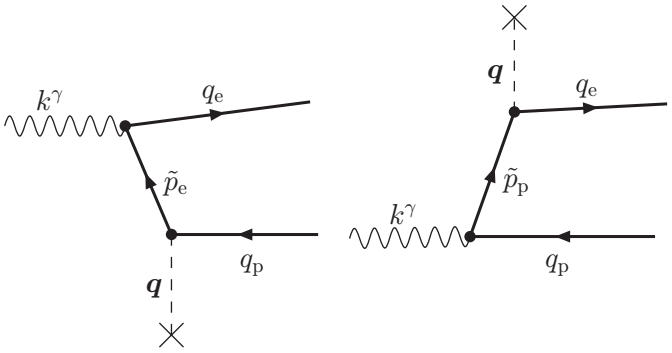

Figure 1. Feynman diagrams describing the process of laser-assisted pair creation. Laser-dressed fermions are denoted by thick lines. The electron effective four momentum in the laser field is q_e, and the laser-dressed positron has an effective momentum q_p. The momentum of the virtual state in the laser-dressed propagator is $\tilde{p}_{\mathrm{e,p}}$. The virtual Coulomb photon with spatial momentum $\boldsymbol{q}$ is drawn as a dashed line, and the absorbed high-energy photon with momentum k^γ as a wavy line. The direction of time is from left to right.

Also the creation of virtual, unobservable electron–positron pairs, produces observable effects, such as photon–photon scattering [32]–[35], photon splitting [36] and photon merging [37].

In this paper, we investigate the possibility to create pairs from vacuum in the presence of three external fields: a laser field, a Coulomb field and a single photon, whose frequency exceeds the pair production threshold. All calculations are performed in the rest frame of the nucleus. In contrast to [38], where the same process was considered for a gamma photon and a laser beam propagating in the same direction, we here consider a different geometry: counterpropagating gamma photon and laser wave. We also consider a different regime for the laser parameters. The fact that the gamma photon and the laser photons propagate in different directions renders the numerical treatment of the problem more complex compared to the setup in [38], but also more interesting theoretically. Employing the full formula, including the fully laser-dressed Dirac–Volkov propagator, allows us, in principle, to treat the general situation where the laser beam and the gamma photon cross at an arbitrary angle. For comparison, one example where the photon and laser beams cross at right angles is therefore included.

The relevant Feynman diagrams are shown in figure 1. The matrix element for this process was first calculated by Roshchupkin [39], and also by Borisov *et al* in [40, 41]; however, without performing any concrete numerical evaluations. The matrix element has a crossing symmetry with the one for laser-assisted bremsstrahlung, which was studied previously in many papers, including [42], and by us recently in [43, 44].

In our case, pair production is possible in the absence of the laser field through the Bethe–Heitler process [45], because we assume the angular frequency ω^γ of the single photon to be larger than the threshold $2m$ (we denote the frequency of the single photon by a superscript rather than a subscript in view of a rather large number of Lorentz subscripts that we will need to introduce in the analysis later). The presence of the laser will then modify the process, so that we can speak about laser-assisted pair production. By contrast, if $\omega^\gamma < 2m$, the laser field would not really assist; it would be necessary even to produce any pairs at all, and we would call the process laser-induced rather than just laser-assisted.

We note the general observation [46] that to produce an appreciable number of pairs, the electric field in the rest frame of the nucleus has to exceed the critical field. We thus expect that for a subcritical field, the *total* rate of laser-assisted pair production will be essentially unaffected by the laser field. In particular, the total cross section is expected to be very small for a subcritical field and $\omega^\gamma < 2m$, where the Bethe–Heitler rate vanishes identically. However, the *differential* cross section, that is, the dependence of the cross section on the directions and energies of the produced particles, can change drastically. In particular, we find that the laser field tends to reverse the direction of the emitted pairs, so that they are produced preferentially in the propagation direction of the laser field, the more so with rising laser intensity. The effect persists also for the case when the gamma photon and laser beam cross at right angles. In comparing the various directions of the laser beam relative to the gamma photon beam, we point out the most favourable geometrical setup for focusing the angular distribution of the created pair. We furthermore show that the angular distribution calculated with the full quantum formula can be explained from the classical motion of the electron and positron in the laser field, if the field-free cross section is utilized as initial distribution. An interesting directional dependence of the maximal energy obtained by the produced pair is also discussed.

The paper is organized as follows. In section 2, we introduce the theory necessary to describe the laser-assisted process, including Volkov states and the Dirac–Volkov propagator, leading to the expression for the S-matrix elements. Next, we present numerical results together with a detailed discussion in section 3.

2. Theory

In this section, we review the theory used to describe laser–matter interaction. The interaction of the electron and positron with the laser field will be treated nonperturbatively, whereas the interaction with the high-frequency photon field and the Coulomb field is taken into account by the first-order perturbation theory.

2.1. Volkov wave functions and propagator

We start from the Dirac equation coupled to an external plane electromagnetic wave $A_\mu(\phi)$:

$$(\mathrm{i}\hat{\partial} - e\hat{A}(\phi) - m)\psi(x) = 0, \tag{1}$$

where $\phi = k_\mu x^\mu$ is the phase of the wave, and $k_\mu = (\omega, \boldsymbol{k})$ is the wave vector. Scalar products will be written with a dot as $a \cdot b = a_\mu b^\mu = a_0 b^0 - \boldsymbol{a} \cdot \boldsymbol{b}$, and a hat denotes the contraction with the Dirac gamma matrices: $\hat{A} = \gamma^\mu A_\mu$. The solution to equation (1) is the well-known Volkov solution [47] and reads

$$\psi_\mp(x) = \sqrt{\frac{m}{Q}}\left(1 \mp \frac{e\hat{A}\hat{k}}{2k \cdot p}\right) u_\mathrm{p}^\mp \exp\left[\mathrm{i}S_\mp(x, p)\right], \tag{2}$$

where

$$S_\mp(x, p) = \mp p \cdot x - \int_0^\phi \left(\frac{e\, p \cdot A(\phi')}{k \cdot p} \mp \frac{e^2 A^2(\phi')}{2k \cdot p}\right) \mathrm{d}\phi'. \tag{3}$$

Here, $\psi_-(x)$ denotes the electron wave function, and $\psi_+(x)$ is the negative energy wave function, corresponding to the positron. Note that e always denotes the charge of the electron.

The spinor $u_{\rm p}^{\mp}$ satisfies $(\hat{p}\mp m)u_{\rm p}^{\mp}=0$. In the following, we specialize to a monochromatic laser wave of linear polarization,

$$A_\mu(\phi)=a\,\epsilon_\mu\cos(\phi), \tag{4}$$

where $\epsilon_\mu=(0,\boldsymbol{\epsilon})$ is the polarization vector satisfying $\epsilon^2=-1$, $k\cdot\epsilon=0$, and a is the amplitude of the vector potential. The integral in equation (3) can then be performed analytically and reads

$$\begin{aligned}S_\mp(x,p)&=\mp p\cdot x\mp\frac{e^2a^2}{4k\cdot p}\phi-\frac{eap\cdot\epsilon}{k\cdot p}\sin\phi\mp\frac{e^2a^2}{8k\cdot p}\sin(2\phi)\\&=\mp q\cdot x-\alpha\sin\phi\pm\beta\sin(2\phi),\end{aligned} \tag{5}$$

where in the last line we have defined the effective momentum $q_\mu=p_\mu+e^2a^2k_\mu/(4k\cdot p)$, with corresponding effective mass $m_*^2=q^2=m^2+e^2a^2/2$, effective energy $Q=q_0$, and the other parameters are $\alpha=e\,a\,(p\cdot\epsilon)/(k\cdot p)$ and $\beta=-e^2\,a^2/(8k\cdot p)$. Later, when we write down the matrix element we will use the following Fourier decomposition of the wave function (2):

$$\psi_\mp(x)=\sqrt{\frac{m}{Q}}\sum_{s=-\infty}^{\infty}\exp\left(\mp\mathrm{i}q\cdot x-\mathrm{i}sk\cdot x\right)\left(A_0(s,\alpha,\pm\beta)\pm\frac{ea\hat{k}\hat{\epsilon}}{2k\cdot p}A_1(s,\alpha,\pm\beta)\right)u_\mp(p), \tag{6}$$

where the generalized Bessel function $A_0(s,\alpha,\beta)$ is defined as an infinite sum over products of ordinary Bessel functions,

$$A_0(s,\alpha,\beta)=\sum_{n=-\infty}^{\infty}J_{2n+s}(\alpha)J_n(\beta) \tag{7}$$

and for positive integer j

$$A_j(s,\alpha,\beta)=\tfrac{1}{2}\left[A_{j-1}(s-1,\alpha,\beta)+A_{j-1}(s+1,\alpha,\beta)\right]. \tag{8}$$

The generalized Bessel function was first introduced by Reiss [12], and was later studied by several authors [13], [48]–[51].

To write down a second-order matrix element, we also need the Dirac–Volkov propagator $G(x,x')$, which can be expressed in a number of different ways [52]. We use the representation [53, 54]

$$\begin{aligned}G(x,x')&=\int\frac{\mathrm{d}^4p}{(2\pi)^4}\left(1+\frac{e\hat{k}\hat{A}(\phi)}{2k\cdot p}\right)\frac{\hat{p}+m}{p^2-m^2+\mathrm{i}\varepsilon}\left(1+\frac{e\hat{A}(\phi)\hat{k}}{2k\cdot p}\right)\exp\left[\mathrm{i}S_-(x,p)-\mathrm{i}S_-(x',p)\right]\\&=\int\frac{\mathrm{d}^4p}{(2\pi)^4}\sum_{s,s'=-\infty}^{\infty}\left(A_0(s,\alpha,\beta)+\frac{ea\hat{k}\hat{\epsilon}}{2k\cdot p}A_1(s,\alpha,\beta)\right)\frac{\hat{p}-(e^2a^2/4k\cdot p)\hat{k}+m}{p^2-m_*^2+\mathrm{i}\varepsilon}\\&\quad\times\exp\left[-\mathrm{i}p\cdot(x-x')-\mathrm{i}k\cdot(sx-s'x')\right]\left(A_0(s',\alpha,\beta)+\frac{ea\hat{\epsilon}\hat{k}}{2k\cdot p}A_1(s',\alpha,\beta)\right),\end{aligned} \tag{9}$$

where ε is small and positive. In the last equality of (9), we have used the specific form (4) of the vector potential, expanded the propagator into a product of two Fourier series, and finally changed variables $p_\mu\to p_\mu+e^2a^2k_\mu/(4k\cdot p)$. This transformation makes the appearance of the effective mass m_* in the propagator denominator explicit.

2.2. Matrix element and cross section

In our treatment, the final states of the electron and the positron are described by Volkov states, and the Dirac–Volkov propagator is employed for the intermediate, virtual states, i.e. the interaction of all fermions with the laser field is taken into account to all orders. The effect of the Coulomb field of the nucleus and the gamma photon is calculated using the perturbation theory. To this end, we introduce the vector potential $A^{\mathrm{C}}_{\mu}(x)$ of the nucleus with atomic charge number $Z = 1$ (the scaling with Z can later be restored easily) and the vector potential $A^{\gamma}_{\mu}(x)$ of the perturbative photon

$$A^{\mathrm{C}}_{\mu}(x) = \frac{-e\,\delta_{\mu 0}}{4\pi\,|\boldsymbol{x}|}, \qquad A^{\gamma}_{\mu}(x) = \frac{1}{\sqrt{2\omega^{\gamma}}}\,\epsilon^{\gamma}_{\mu}\,\mathrm{e}^{-\mathrm{i}k^{\gamma}\cdot x}. \tag{10}$$

Here, ω^{γ} denotes the frequency and k^{γ}_{μ} the μth component of the momentum four vector of the gamma photon. Note the minus sign in the exponential in $A^{\gamma}_{\mu}(x)$, since photon absorption is the desired process. Expressions (2), (9) and (10) now permit us to write down the matrix element S for the production of one electron with effective momentum q_{e} and one positron with effective momentum q_{p}, by absorption of one photon k^{γ}, corresponding to both Feynman diagrams in figure 1:

$$\begin{aligned}
S &= \sum_{n=-\infty}^{\infty} S_n \delta(Q_{\mathrm{p}} + Q_{\mathrm{e}} + n\omega - \omega^{\gamma}) \\
&= 2\pi\,\mathrm{i} \sum_{n,s=-\infty}^{\infty} \frac{e^3\,m}{\sqrt{2\omega^{\gamma}\,Q_{\mathrm{p}}Q_{\mathrm{e}}}} \frac{\delta(Q_{\mathrm{p}} + Q_{\mathrm{e}} + n\omega - \omega^{\gamma})}{(\boldsymbol{q}_{\mathrm{e}} + \boldsymbol{q}_{\mathrm{p}} + n\,\boldsymbol{k} - \boldsymbol{k}^{\gamma})^2} \\
&\quad \times \bar{u}^{-}_{p_{\mathrm{e}}} \Bigg(F^{s}_{4334}(\hat{\epsilon}^{\gamma}) \frac{\hat{\tilde{p}}_{\mathrm{e}} - \hat{k}e^2a^2/(4k\cdot\tilde{p}_{\mathrm{e}}) + m}{\tilde{p}^2_{\mathrm{e}} - m^2_{*}} F^{s-n}_{1313}(\gamma^0) \\
&\quad + F^{s+n}_{4224}(\gamma^0) \frac{\hat{\tilde{p}}_{\mathrm{p}} - \hat{k}e^2a^2/(4k\cdot\tilde{p}_{\mathrm{p}}) + m}{\tilde{p}^2_{\mathrm{p}} - m^2_{*}} F^{s}_{1212}(\hat{\epsilon}^{\gamma}) \Bigg) u^{+}_{p_{\mathrm{p}}},
\end{aligned} \tag{11}$$

where

$$\begin{aligned}
F^{m}_{KLMN}(X) &= A_0(m, \alpha_K - \alpha_L, \beta_K - \beta_L)X \\
&\quad + A_1(m, \alpha_K - \alpha_L, \beta_K - \beta_L) \left(\frac{Xea\hat{k}\hat{\epsilon}}{2k\cdot p_M} + \frac{ea\hat{\epsilon}\hat{k}X}{2k\cdot p_N} \right) \\
&\quad + A_2(m, \alpha_K - \alpha_L, \beta_K - \beta_L) \frac{e^2\hat{a}\hat{k}X\hat{k}\hat{a}}{4k\cdot p_M k\cdot p_N},
\end{aligned} \tag{12}$$

with $K, L, M, N \in \{1, 2, 3, 4\}$, $X \in \{\hat{\epsilon}^{\gamma}, \gamma^0\}$,

$$\alpha_K = ea\epsilon\cdot p_K/(k\cdot p_K), \qquad \beta_K = -e^2a^2/(8k\cdot p_K), \tag{13}$$

$p_1 = -q_{\mathrm{p}}$, $p_2 = \tilde{p}_{\mathrm{p}} = -q_{\mathrm{p}} + sk + k^{\gamma}$, $p_3 = \tilde{p}_{\mathrm{e}} = q_{\mathrm{e}} + sk - k^{\gamma}$ and $p_4 = q_{\mathrm{e}}$. We recall that index e (p) is used to label the electron (positron) momentum vector. Expression (11) was first obtained in [39]. The first line in equation (11) implicitly defines the nth-order matrix element S_n, and the argument of the delta function in equation (11) expresses energy conservation in terms of the effective energies Q_{p} and Q_{e}. The number $-n$ ($+n$) can be interpreted as the number of photons absorbed from (emitted into) the laser mode during the process. In particular,

the threshold $\omega^\gamma - n\omega \geqslant 2m_*$ for pair creation is higher than the field-free case, due to the larger effective mass $m_* > m$. We further remark that in contrast to the case with copropagating gamma photon and laser field [38], where the condition $k^\gamma \cdot k = 0$ provides for a considerable simplification of the matrix element (11), the present case with $k^\gamma \cdot k \neq 0$ requires the full expression (11). In particular, all terms in the sum over s have to be included, which renders the numerical evaluation of the differential cross section rather demanding. From the matrix element, we obtain by the usual methods [55] the differential cross section $\mathrm{d}\sigma$, averaged over the polarization of the gamma photon and summed over the spins of the electron and positron:

$$\begin{aligned}\mathrm{d}\sigma &= \frac{1}{2}\sum_{\text{spin,pol.}} \frac{\mathrm{d}^3q_\mathrm{p}}{(2\pi)^3}\frac{\mathrm{d}^3q_\mathrm{e}}{(2\pi)^3}\,|S|^2\,\frac{1}{T}\\ &= \frac{1}{4\pi}\sum_{\text{spin,pol.},\,n} \frac{\mathrm{d}^3q_\mathrm{p}}{(2\pi)^3}\frac{\mathrm{d}^3q_\mathrm{e}}{(2\pi)^3}|S_n|^2\delta(Q_\mathrm{p}+Q_\mathrm{e}+n\omega-\omega^\gamma),\end{aligned} \tag{14}$$

where in the last line the delta function is explicitly written out. The matrix element (11) is gauge invariant, both under the gauge transformation $\epsilon_\mu \to \epsilon_\mu + C_1 k_\mu$ of the laser field and $\epsilon^\gamma_\mu \to \epsilon^\gamma_\mu + C_2 k^\gamma_\mu$, where $C_{1,2}$ are constants. Gauge invariance, especially for the gamma photon field, provides a sensible numerical check of the computer code used to evaluate the differential cross section (14).

Another numerical test of correctness is the behaviour of the cross section at the apparent singularity when $k\cdot\tilde{p}_{\mathrm{e,p}} \to 0$ in the F functions in the expression on the right-hand side of equation (11) (we recall that $p_2 = \tilde{p}_\mathrm{p}$ and $p_3 = \tilde{p}_\mathrm{e}$). The matrix element can be shown to be finite in this limit, but the calculation constitutes a test of numerical stability as the arguments of the generalized Bessel functions tend to infinity.

3. Results and discussion

In this section, we present results of a concrete numerical evaluation of the differential cross section (14). The frequency of the laser is taken to be $\omega = 1$ keV, and the amplitude a is chosen such that the classical nonlinearity parameter $\xi = -ea/m$ is of order unity. Experimentally, this choice of parameters can be realized in either of the two following scenarios. For a high-power laser, operating at a photon energy of 1 eV and intensity of $9\times10^{17}\,\mathrm{W\,cm^{-2}}$, head-on collision with a relativistic nucleus with a Lorentz boost factor $\gamma \approx 500$ will give $\xi = 1$ and $\omega = 1$ keV in the rest frame of the nucleus. In an alternative scenario, a focused x-ray free-electron laser [56] applied to a nucleus at rest may also give access to the parameters above. Here $\xi = 1$ and $\omega = 1$ keV in the laboratory frame requires an intensity of $9\times10^{23}\,\mathrm{W\,cm^{-2}}$ at the focus of the laser. In this regime, the peak electric field of the laser is still much smaller than the critical field, $E_\mathrm{peak}/E_\mathrm{c} = \xi\omega/m \ll 1$. In view of the admittedly high laser frequency ω, we note that we expect the results presented here to be insensitive to ω (at fixed ξ), as long as we have $\xi\omega/m \ll 1$. We will mostly consider the case where the laser counterpropagates with the gamma photon, and describe the direction of the produced electron and positron by an angle $\theta_{\mathrm{e,p}}$, as depicted in figure 2(a). Also examples where the gamma photon and laser photons copropagate, depicted in figure 2(b), and where $\boldsymbol{k}$ and $\boldsymbol{k}^\gamma$ are perpendicular to each other, as shown in figure 2(c), will be discussed.

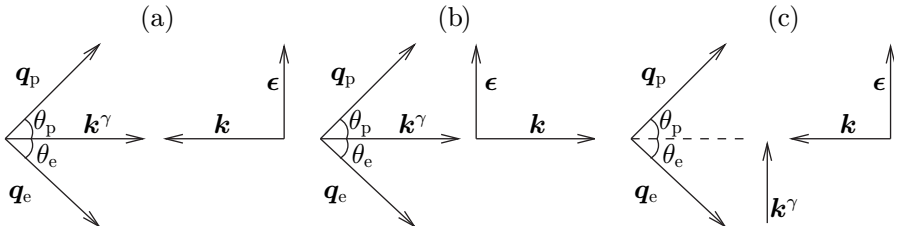

Figure 2. The geometrical setup of the considered process, defining the angles θ_p and θ_e. (a) Gamma photon and laser beam counterpropagating. (b) Gamma photon and laser beam copropagating. (c) Gamma photon and laser beam cross at right angles. The gamma photon has three-momentum $\boldsymbol{k}^\gamma$, the laser field has wave vector $\boldsymbol{k}$ and polarization vector $\boldsymbol{\epsilon}$, the positron has effective three-momentum $\boldsymbol{q}_p$, and the electron has effective three-momentum $\boldsymbol{q}_e$. The vectors $\boldsymbol{q}_p$ and $\boldsymbol{q}_e$ lie in the plane spanned by $\boldsymbol{k}$ and $\boldsymbol{\epsilon}$.

3.1. Energy cutoff

In principle, since the sum over n in equation (11) extends from $-\infty$ to $+\infty$, the created pair can acquire arbitrarily high effective energies Q_p and Q_e. This should be compared with the field-free case, given by the Bethe–Heitler formula [45], where the cross section vanishes identically for positron (or electron) energies $E > \omega^\gamma - m$. In practice, however, an apparent cutoff will occur in the energy spectrum, and thereby limit the available energy for the produced pair. In the following, we will assume the directions $\boldsymbol{q}_e/|\boldsymbol{q}_e|$, $\boldsymbol{q}_p/|\boldsymbol{q}_p|$ of the positron and electron given, and consider the differential cross section (14) as a function of the effective energy Q_p of the positron. The effective energy Q_e of the electron is fixed by energy conservation for each n. It follows from expression (11) that to find the energy cutoff, we should consider the behaviour of the function

$$H_n = \sum_{s=-\infty}^{\infty} \frac{A_0(s, \alpha_e - \tilde{\alpha}, \beta_e - \tilde{\beta})}{s + C} A_0(s - n, \alpha_p - \tilde{\alpha}, \beta_p - \tilde{\beta}) \tag{15}$$

as a function of n. As follows from the discussion in section 3.2, we can assume that C is a noninteger. As shown in appendix A, function (15) has the same cutoff properties as the generalized Bessel function

$$A_0(n, \alpha_e - \alpha_p, \beta_e - \beta_p), \tag{16}$$

provided C is larger than the cutoff index of the first of the A_0 in the numerator in equation (15). As $\beta_e - \beta_p = -[(k \cdot q_e)^{-1} + (k \cdot q_p)^{-1}]\, e^2 a^2/8 < 0$, and high values of Q_p are obtained by absorbing photons, that is, for negative n, it follows that Q_p^{cutoff} is the largest positron energy for which the inequality

$$n_{\text{pos.cutoff}} > |n| \tag{17}$$

is still satisfied. The integer $n_{\text{pos.cutoff}}$ is defined in equation (A.1). Since the quantities $k \cdot q_e$ and $k \cdot q_p$ involve direction cosines, it becomes clear that the energy cutoff is direction-dependent. In particular, this implies that the maximal energy Q_p^{cutoff} will depend not only on the direction of the positron, but also on the direction of the electron. In order to determine the direction-dependent energy cutoff, one therefore proceeds as follows. In the first step, one fixes the directions of the electron and positron, which define $n_{\text{pos.cutoff}}$ as a function of n and Q_p. In

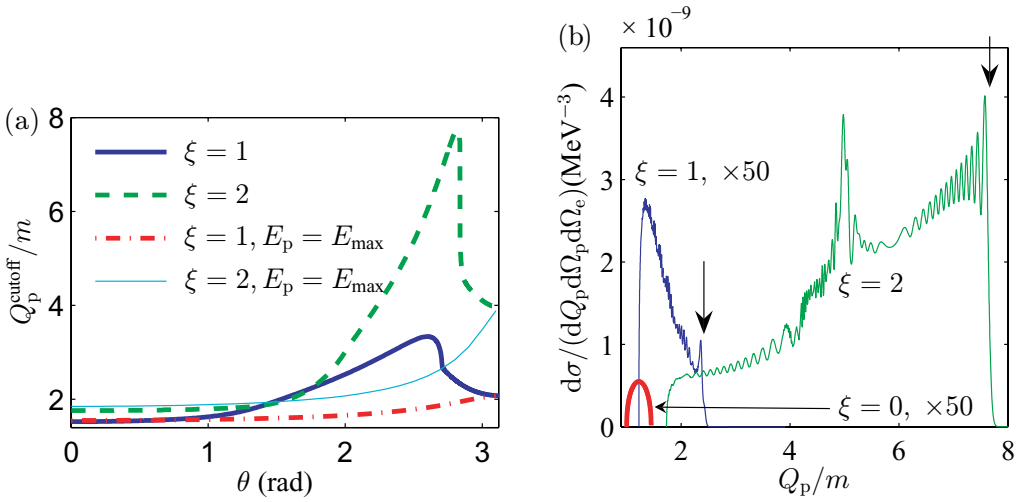

Figure 3. (a) Effective energy cutoff as a function of the angle $\theta = \theta_p = \theta_e$ in the counterpropagating setup (figure 2(a)), resulting from the solution of equation (17). For comparison, we also show the effective energy that would result if the positron were created with the largest available energy in the absence of the laser, $E_p = E_{max} = \omega^\gamma - m$, and then placed in the laser field with fixed direction of $\boldsymbol{q}_p$ (all curves are labelled accordingly). The difference of the latter two curves to the laser-dressed solution is because of the correlation between the electron and positron induced by the laser. This kind of correlation was also observed in [22]. In (b), we show a concrete example of the cross section, for $\theta = 2.8$ rad in the counterpropagating setup, chosen to maximize the cutoff for $\xi = 2$. The 'laser-assisted' curves show complex oscillatory behaviour, with a peak just before the cutoff. The cutoffs predicted by equation (17) are indicated by arrows. Note that the curves for $\xi = 1$ and 0 were multiplied by a factor 50; the ordinate axis is kept on a linear scale.

the second step, one varies Q_p and in this way finds the largest positron effective energy Q_p satisfying equation (17).

As a concrete example, we let the positron and electron be ejected at equal angles $\theta_p = \theta_e \equiv \theta$ in the counterpropagating setup (figure 2(a)), and show in figure 3 the cutoff as a function of θ for different values of the intensity parameter ξ. The frequency of the single photon is $\omega^\gamma = \sqrt{6}\,m$, which corresponds exactly to the threshold value $2m_*$ for $\xi = 1$. In the same figure, we also show a concrete evaluation of the differential cross section for the corresponding parameters, compared with the laser-free case. The magnitude of the differential cross section is here significantly larger than the case without the laser, and also displays complicated oscillatory behaviour.

3.2. Resonances and competing processes

In principle, the matrix element (11) diverges if one of the intermediate momenta $\tilde{p}_e$, $\tilde{p}_p$ satisfies the on-shell condition

$$\tilde{p}_e = (q_e + sk - k^\gamma)^2 = m_*^2, \qquad \tilde{p}_p = (k^\gamma - q_p + sk)^2 = m_*^2 \tag{18}$$

for some integer s. Physically speaking, this means that the considered second-order process splits up into two consecutive first-order processes, laser-induced pair creation by a gamma photon followed by Coulomb scattering of the electron or the positron. This phenomenon has been studied before in the context of laser-assisted electron–electron scattering [57]–[59] and laser-assisted bremsstrahlung [42]–[44], [60]. The usual way to regularize the matrix element, so that it remains finite also at condition (18), is to add a small imaginary part to the energy of the electron (positron) [61], related to the total probability for the intermediate state to decay by Compton scattering. Finite values will also result if the finite extent of the laser field or the frequency width of the laser or photon beam is taken into account. In the current paper, however, we consider a regime of parameters where the resonances are strongly suppressed. Mathematically, this means that the value of s needed to satisfy the resonance condition (18) is larger than the corresponding cutoff index for the generalized Bessel function, and that the contribution from this index in the sum over s is negligible, once properly regularized. Physically speaking, we are dealing with laser parameters such that purely laser-induced processes, that cannot occur in the absence of the laser, have vanishingly small probability to occur. The basic requirement for laser-induced processes like pair creation by a photon [13] (at photon frequency $\omega^\gamma \approx 2m$) or pair creation by a nucleus [16] to have substantial probability is that the peak electric field $E_{\mathrm{peak}} = a\omega$ should be comparable with the critical field, $E_{\mathrm{peak}}/E_{\mathrm{c}} \approx 1$, and, as mentioned before, we consider only laser parameters a, ω such that $E_{\mathrm{peak}} \ll E_{\mathrm{c}}$. This also means that at the field strengths considered, there are no competing processes, so that our process will indeed be the dominant one.

3.3. Angular distribution

For the field-free case, the pairs prefer to emerge at an angle $\theta \sim m/\omega^\gamma$ with the vector $\boldsymbol{k}^\gamma$ [45]. When the laser field is turned on, we expect to find more pairs in the direction of the laser wave vector $\boldsymbol{k}$. In figure 4, we display the differential cross section integrated over $\mathrm{d}Q_{\mathrm{p}}$ and $\mathrm{d}Q_{\mathrm{e}}$, for $\xi = 1, 2$. The peak is seen to shift from the direction of the gamma photon to the direction of the laser wave.

In figure 5, we consider for comparative purposes a different setup: here we let the gamma photon beam and the laser beam cross at right angles, so that $\boldsymbol{k} \cdot \boldsymbol{k}^\gamma = 0$. The angles for the positron and electron are defined in the same way as before, so that $\theta = \theta_{\mathrm{e}} = \theta_{\mathrm{p}}$, with $\cos\theta = -\boldsymbol{q}_p \cdot \boldsymbol{k}/(\omega|\boldsymbol{q}_{\mathrm{p}}|)$ (see figure 2(c)). As expected, the laser-assisted angular distribution is distorted compared with the rather broad field-free distribution. Comparing the three relative directions of laser beam and gamma photon beam (figures 4 and 5), we see that the setup most favourable for focusing of the created pair is when the laser photons and the gamma photon propagate in the same direction, shown in figure 4(b). In this case, the laser field considerably narrows the angular distribution, so that the pair is ejected into a much smaller solid angle, compared with the field-free cross section. An intuitive explanation for this conclusion is offered below.

Interestingly, the angular distribution can be explained from the classical motion of the electron and positron in the laser field, with the Bethe–Heitler cross section as the initial momentum distribution. To this end, assume that the particle (electron or positron) with mass m and charge e, is created instantaneously by the Bethe–Heitler process with initial momentum p_0^μ at laser phase ϕ_0. This should be a good approximation since the creation process is expected to take place on a scale comparable to the Compton wavelength $\lambda_{\mathrm{C}} = 1/m \ll 1/\omega$, much

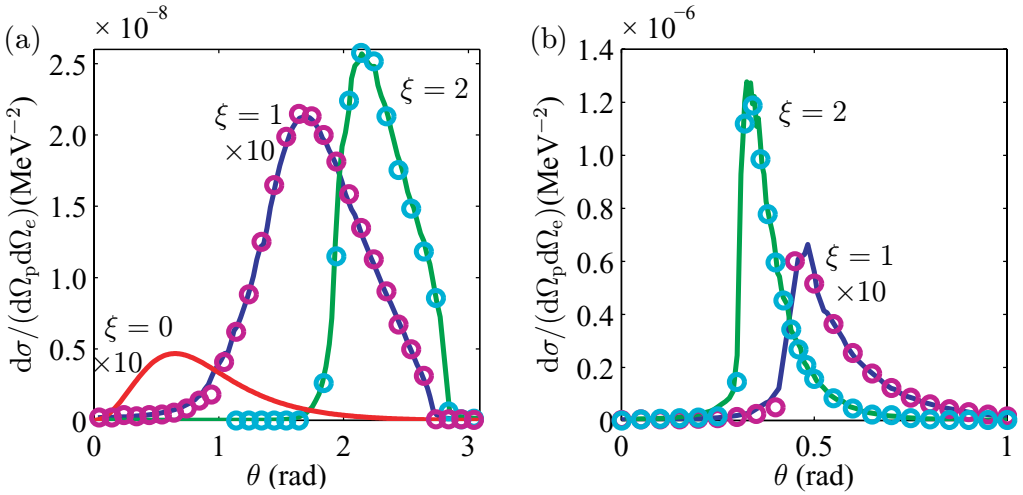

Figure 4. (a) Counterpropagating setup (figure 2(a)): the differential cross section integrated over the effective energy $Q_{p,e}$, for $\xi = 0$ (solid red line), $\xi = 1$ (solid blue line: quantum formula (14), circles: classical approximation (22)) and for $\xi = 2$ (solid green line: quantum, circles: classical). For transformation to other frequently employed units for the cross section one uses $\mathrm{MeV}^{-2} = 389\,\mathrm{b} = 389 \times 10^{-24}\,\mathrm{cm}^2$. As in figure 3, $\omega^\gamma = \sqrt{6}\,m$. The pair is emitted at equal angles $\theta_p = \theta_e = \theta$ (see figure 2), in the plane spanned by $\boldsymbol{k}$ and $\boldsymbol{\epsilon}$. In the geometry of counterpropagating gamma photon and laser beam, the direction $\theta = 0$ corresponds to the gamma photon propagation direction, whereas $\theta = \pi$ indicates the propagation direction of the laser field. The curves for $\xi = 0$ and 1 were multiplied by a factor of 10. We note that the area under these curves is notably different, which implies that the presence of the laser enhances the number of pairs produced at $\theta_p = \theta_e$. The differential cross section integrated over all angles is however, as we will see later (see figure 6), almost unchanged as compared with the laser-free case. For comparison, we show in panel (b) the case where the laser beam and gamma photon beam are copropagating (figure 2(b)), so that $\theta = 0$ corresponds to the direction of both gamma photon and laser beam. The parameters are otherwise unchanged. The $\xi = 0$ curve is the same as in (a) and therefore not shown. In this case, the peaks are much sharper, due to the combined effect of the gamma photon and the laser beam. Also in the copropagating case, as verified in [38], the total cross section is the same as the field-free cross section.

smaller than the laser wavelength. According to the classical, relativistic equations of motion for a charged particle in a plane electromagnetic wave with vector potential given in (4), the momentum p^μ at a later phase ϕ reads [62]

$$p^\mu = p_0^\mu + \frac{ea\epsilon \cdot p_0}{k \cdot p_0}(\cos\phi - \cos\phi_0)k^\mu + \frac{e^2a^2}{2k \cdot p_0}(\cos\phi - \cos\phi_0)^2 k^\mu - ea(\cos\phi - \cos\phi_0)\epsilon^\mu. \tag{19}$$

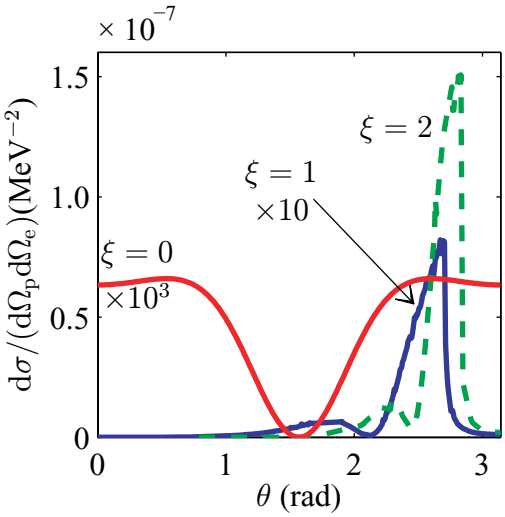

Figure 5. Differential cross section integrated over Q_p, for the case where the propagation direction of the gamma photon is perpendicular to the propagation direction of the laser field, $\boldsymbol{k}\cdot\boldsymbol{k}^\gamma = 0$ (figure 2(c)). Here $\theta = \pi$ corresponds to emission of the pair in the direction of the laser photons. The parameters are otherwise identical to those employed in figure 4. The curve for $\xi = 0$ was multiplied with a factor 10^3, and the curve for $\xi = 1$ was multiplied with a factor 10.

Averaging over ϕ yields the effective momentum q^μ:

$$q^\mu = p_0^\mu - \frac{ea\epsilon\cdot p_0}{k\cdot p_0}\cos\phi_0 k^\mu + \frac{e^2a^2}{2k\cdot p_0}\left(\cos^2\phi_0 + \frac{1}{2}\right)k^\mu + ea\cos\phi_0\epsilon^\mu. \tag{20}$$

Here an important remark is that $k\cdot q = k\cdot p = k\cdot p_0$, and that (20) is independent of ω. The final effective momentum thus depends on the laser phase when the particle was created. Conversely, given a final effective momentum q and a phase ϕ_0, the initial momentum $p_0(q,\phi_0)$ follows. Now, assuming the initial electron and positron momenta $p_{\mathrm{e}0}$, $p_{\mathrm{p}0}$ to be distributed according to the Bethe–Heitler differential cross section $\mathrm{d}\sigma^{\mathrm{BH}}/(\mathrm{d}^3p_\mathrm{e}\,\mathrm{d}^3p_\mathrm{p}) \equiv f^{\mathrm{BH}}(p_\mathrm{e},p_\mathrm{p})$ [45], the classically laser-modified cross section $\mathrm{d}\sigma^{\mathrm{class.}}/(\mathrm{d}^3q_\mathrm{e}\,\mathrm{d}^3q_\mathrm{p})$ is obtained by averaging over the initial phase,

$$\frac{\mathrm{d}\sigma^{\mathrm{class.}}}{\mathrm{d}^3q_\mathrm{e}\,\mathrm{d}^3q_\mathrm{p}} = \frac{1}{2\pi}\int_0^{2\pi}\mathrm{d}\phi_0 f^{\mathrm{BH}}\left(p_{\mathrm{e}0}(q_\mathrm{e},\phi_0), p_{\mathrm{p}0}(q_\mathrm{p},\phi_0)\right)\frac{\partial\boldsymbol{p}_{\mathrm{e}0}}{\partial\boldsymbol{q}_\mathrm{e}}\frac{\partial\boldsymbol{p}_{\mathrm{p}0}}{\partial\boldsymbol{q}_\mathrm{p}}, \tag{21}$$

where $(\partial\boldsymbol{p}_{\mathrm{e}0}/\partial\boldsymbol{q}_\mathrm{e})(\partial\boldsymbol{p}_{\mathrm{p}0}/\partial\boldsymbol{q}_\mathrm{p})$ is the Jacobian. Integrating over Q_p and Q_e, we arrive at the cross section differential in the solid angles of the electron and positron:

$$\frac{\mathrm{d}\sigma^{\mathrm{class.}}}{\mathrm{d}\Omega_\mathrm{e}\,\mathrm{d}\Omega_\mathrm{p}} = \int_{m_*}^\infty \mathrm{d}Q_\mathrm{e}\int_{m_*}^\infty \mathrm{d}Q_\mathrm{p}\frac{\mathrm{d}\sigma^{\mathrm{class.}}}{\mathrm{d}^3q_\mathrm{e}\,\mathrm{d}^3q_\mathrm{p}}Q_\mathrm{e}|\boldsymbol{q}_\mathrm{e}|Q_\mathrm{p}|\boldsymbol{q}_\mathrm{p}|. \tag{22}$$

The cross section (22) is plotted with circles in figure 4, as a comparison to the full quantum formula (14). The agreement is very good, confirming the picture that the pairs are instantaneously created by the gamma photon, and subsequently accelerated by the laser field as classical particles.

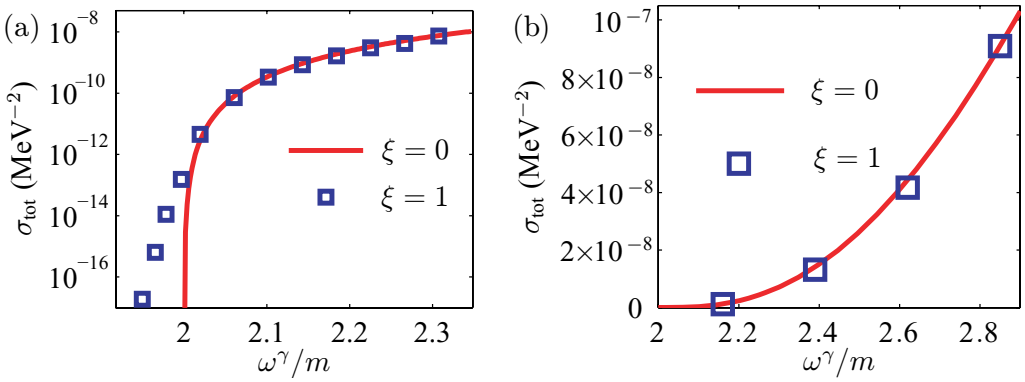

Figure 6. The total cross section as a function of the frequency ω^γ of the nonlaser mode photon, compared with the case without the laser field. (a) Logarithmic scale, close to threshold. (b) Linear scale, for larger ω^γ. The laser frequency used is $\omega = 1$ keV. Due to the laser, there remains a finite probability of pair creation below the field-free threshold $\omega^\gamma = 2m$. However, the magnitude drops exponentially, as expected.

From the above arguments, the intuitive picture of why the angular distribution is distorted by the laser field compared to the field-free case is clear: in addition to the initial momentum from the created gamma photon, the positron (or electron) receives an additional momentum kick by the laser field. Since the momentum transfer in the laser propagation direction grows with the laser field strength as ξ^2, compared to ξ in the polarization direction (see equation (20)), it follows that the tendency for the pair to be ejected in the propagation direction grows with ξ, or the field strength of the laser. The width of the distribution is largest for $\xi = 1$ in figure 4(a), because in this regime the momentum transfers in the laser propagation direction from the laser field, $p^\parallel_{\rm laser}$, and from the gamma photon, $p^\parallel_0$, are comparable and opposite, so that the net momentum transfer $p^\parallel_{\rm laser} + p^\parallel_0$ is rather small. A quantitative estimate yields $p^\parallel_{\rm laser} = \xi^2 m^2 \omega/(2k \cdot p_0) \approx 0.3\xi^2\, m$, and $p^\parallel_0 \approx -0.4m$ for the energy $E_0 = \omega^\gamma/2 = \sqrt{6}m/2$ and the angle $\theta = 1$. This results, for $\xi = 1$ in figure 4(a), in a broad distribution where neither the laser photon direction nor the gamma photon direction is preferred as ejection direction. In contrast, in figure 4(b), where the copropagating setup is shown, the transferred momenta from the gamma photon and from the laser photons along $\boldsymbol{k}$ point in the same direction, $p^\parallel_0 \approx 0.4m$ and $p^\parallel_{\rm laser} = \xi^2 m^2 \omega/(2k \cdot p_0) \approx 0.6\xi^2\, m$ for the same $\boldsymbol{p}_0$ as above, so that the sum is larger than without the laser field, $|p^\parallel_{\rm laser} + p^\parallel_0| > |p^\parallel_0|$. Since the phase-averaged momentum absorbed from the laser beam along $\boldsymbol{\epsilon}$ vanishes, the total momentum component along $\boldsymbol{\epsilon}$ is given by the momentum $p^\perp_0$ from the gamma photon. The final angle $\theta = \arctan[p^\perp_0/(p^\parallel_0 + p^\parallel_{\rm laser})]$ in figure 4(b) is therefore essentially smaller compared with the laser-free case, and consequently a narrower angular distribution follows.

We conclude by the remark that in general the copropagating setup is the most favourable for laser-assisted channelling of the pairs. For practical purposes of measuring the created pair, or creation of, for example, a positron beam, the copropagating setup is thus to be preferred.

3.4. Total cross section

The total cross section is obtained by integrating the differential cross section (14) over the energies Q_p, Q_e, and solid angles Ω_e, Ω_p of the produced positron and electron:

$$\sigma_\mathrm{tot} = \int \frac{1}{4\pi} \sum_{\text{spin, pol., } n} \frac{Q_\mathrm{p}|\boldsymbol{q}_\mathrm{p}|\mathrm{d}Q_\mathrm{p}\mathrm{d}\Omega_\mathrm{p}}{(2\pi)^3} \frac{Q_\mathrm{e}|\boldsymbol{q}_\mathrm{e}|\mathrm{d}Q_\mathrm{e}\mathrm{d}\Omega_\mathrm{e}}{(2\pi)^3} |S_n|^2 \delta(Q_\mathrm{p} + Q_\mathrm{e} + n\omega - \omega^\gamma). \tag{23}$$

Here, it is convenient to replace the sum over the number of exchanged photons n by an integral, and to evaluate this integral with the delta function so that n equals the integer closest to $(\omega^\gamma - Q_\mathrm{p} - Q_\mathrm{e})/\omega$. This is a good approximation since $\omega \ll Q_\mathrm{e,p}, \omega^\gamma$. The remaining six-fold integral has to be performed numerically (we employ a Monte Carlo method). We note that this method has been used before to obtain total rates for the production of pairs from a colliding laser beam and a nucleus [25, 26]. In general, Monte Carlo integration is the method of choice for integrals of high dimensionality where the accuracy demand is modest. The result of one such calculation, for the counterpropagating setup, is shown in figure 6, where we present the total cross section as a function of the frequency ω^γ of the perturbative photon. As expected, in the region where pair production is possible without the laser, the rates are almost indistinguishable.

4. Conclusions

In this paper, we have presented calculations of the laser-assisted Bethe–Heitler process, i.e. pair production by a high-frequency photon in the presence of a nuclear Coulomb field and an intense laser field. The regime of parameters considered was for a subcritical laser field, that is the peak electric field of the laser was much smaller than the critical field $E_\mathrm{c} = m^2/|e|$, but with the nonlinear parameter ξ of order unity and the gamma photon frequency $\omega^\gamma > 2m$. In this regime, pair production is possible without the field, and as the laser field strength is below the critical field, it is expected that the total rates are almost unaffected by the laser. This was confirmed by evaluating the six-fold integral for the total cross section numerically (see figure 6). However, the differential cross section was found to be drastically altered by the presence of the laser wave, as shown in figures 4 and 5. For practical purposes, the copropagating setup is concluded to be superior, although drastic enhancement of the pair production is also predicted for the counterpropagating setup and the setup 'at right angles', provided the detection of the pairs is restricted to a narrow angular region (see figures 4 and 5). Finally, we note that all cross sections shown here are evaluated for a nuclear charge number $Z = 1$ and scale as Z^2, since we have taken into account the Coulomb field in first-order perturbation theory.

Clear laser-assisted signatures are thus expected in the differential cross sections, and these might provide an opportunity for interesting experiments in the near future.

Acknowledgments

We thank A Di Piazza for useful discussions. One of the authors (UDJ) acknowledges support by the Deutsche Forschungsgemeinschaft (Heisenberg program).

Appendix A. Cutoff properties of the generalized Bessel functions

Important for the understanding of physical processes expressed through generalized Bessel functions is the cutoff behaviour. A rule is needed for how many terms should be included in sums like equation (11) to reach convergence. For the ordinary Bessel function $J_n(\alpha)$, the cutoff rule is well known: for $n > \alpha$ (positive n, α) the magnitude of $J_n(\alpha)$ will drop sharply as $J_n(\alpha) \sim \alpha^n / n^{n+(1/2)}$, and the cutoff is therefore $n \approx \alpha$. For the generalized Bessel function $A_0(n, \alpha, \beta)$, the correct rule reads for positive α and β:

$$n_{\text{pos.cutoff}} = \begin{cases} \alpha - 2\beta, & \text{if} \quad 8\beta < \alpha, \\ 2\beta + \dfrac{\alpha^2}{16\beta}, & \text{if} \quad 8\beta > \alpha, \end{cases} \tag{A.1}$$

$$n_{\text{neg.cutoff}} = -\alpha - 2\beta. \tag{A.2}$$

For negative α and β we use the symmetries

$$\begin{aligned} A_0(n, \alpha, -\beta) &= (-1)^n A_0(-n, \alpha, \beta), \\ A_0(n, -\alpha, \beta) &= (-1)^n A_0(n, \alpha, \beta). \end{aligned} \tag{A.3}$$

Beyond the cutoff, $|A_0(n, \alpha, \beta)|$ will show inverse factorial decrease $\sim n^{-|n|}$, similar to $J_n(\alpha)$. These cutoff rules can be derived from the asymptotic expansion by the saddle point method [13, 48, 63] or from the maximal and minimal values of the classically allowed energy for an electron moving in a plane electromagnetic wave [62].

Regarding the function H_n, as appeared in equation (15)

$$H_n = \sum_{s=-\infty}^{\infty} \frac{A_0(s, \alpha, \beta)\, A_0(s - n, \gamma, \delta)}{s + C}, \tag{A.4}$$

we can use the expansion

$$\frac{1}{s + C} = \frac{1}{C} - \frac{s}{C^2} + \frac{s^2}{C^3} + \cdots \tag{A.5}$$

and then perform the sum over s with the addition theorem for generalized Bessel functions, for each term in expansion (A.5). Provided C is larger than the cutoff index of the first of the generalized Bessel functions entering the sum in equation (A.4), we can then write

$$H_n(\alpha, \beta, \gamma, \delta) = \frac{A_0(n, \alpha - \gamma, \beta - \delta)}{C} + \frac{W_2(n, \alpha, \beta, \gamma, \delta)}{C^2} + \frac{W_3(n, \alpha, \beta, \gamma, \delta)}{C^3} + \cdots. \tag{A.6}$$

We also give the expression for the first correction W_2:

$$\begin{aligned} W_2(n, \alpha, \beta, \gamma, \delta) = &-\frac{\alpha}{2}[A_0(n - 1, \Gamma, \Delta) + A_0(n + 1, \Gamma, \Delta)] \\ &+\beta[A_0(n - 2, \Gamma, \Delta) + A_0(n + 2, \Gamma, \Delta)], \end{aligned} \tag{A.7}$$

where $\Gamma = \alpha - \gamma$ and $\Delta = \beta - \delta$. It is now clear that $H_n(\alpha, \beta, \gamma, \delta)$ will have the same cutoff behaviour as $A_0(n, \alpha - \gamma, \beta - \delta)$, under the stated conditions.

References

[1] Sauter F 1931 *Z. Phys.* **69** 742–64
[2] Schwinger J 1951 *Phys. Rev.* **82** 664–79
[3] Brézin E and Itzykson C 1970 *Phys. Rev.* D **2** 1191–9
[4] Popov V S 1971 *Pis'ma Zh. Éksp. Teor. Fiz.* **13** 261–3
Popov V S 1971 *JETP Lett.* **13** 185 (Engl. Transl.)
[5] Popov V S 2001 *Pis'ma Zh. Éksp. Teor. Fiz.* **74** 151–6
Popov V S 2001 *JETP Lett.* **74** 133 (Engl. Transl.)
[6] Baĭer V N, Katkov V M and Strakhovenko V M 1971 *Yad. Fiz.* **14** 1020–6
Baĭer V N, Katkov V M and Strakhovenko V M 1972 *Sov. J. Nucl. Phys.* **14** 572 (Engl. Transl.)
[7] Baĭer V N, Katkov V M and Strakhovenko V M 1991 *Yad. Fiz.* **53** 1021–9
Baĭer V N, Katkov V M and Strakhovenko V M 1991 *Sov. J. Nucl. Phys.* **53** 632 (Engl. Transl.)
[8] Bulanov S S, Narozhny N B, Mur V D and Popov V S 2006 *Zh. Éksp. Teor. Fiz.* **129** 14–29
Bulanov S S, Narozhny N B, Mur V D and Popov V S 2006 *JETP* **102** 9 (Engl. Transl.)
[9] Avetissian H K, Avetissian A K, Mkrtchian G F and Sedrakian K V 2002 *Phys. Rev.* E **66** 016502
[10] Di Piazza A 2004 *Phys. Rev.* D **70** 053013
[11] Blaschke D B, Prozorkevich A V, Roberts C D, Schmidt S M and Smolyansky S A 2006 *Phys. Rev. Lett.* **96** 140402
[12] Reiss H R 1962 *J. Math. Phys.* **3** 59–67
[13] Nikishov A I and Ritus V I 1964 *Zh. Éksp. Teor. Fiz.* **46** 776–96
Nikishov A I and Ritus V I 1964 *Sov. Phys.—JETP* **19** 529 (Engl. Transl.)
[14] Burke D L *et al* 1997 *Phys. Rev. Lett.* **79** 1626–9
[15] Bamber C *et al* 1999 *Phys. Rev.* D **60** 092004
[16] Yakovlev V P 1965 *Zh. Éksp. Teor. Fiz.* **49** 318–28
Yakovlev V P 1965 *Sov. Phys.—JETP* **49** 223 (Engl. Transl.)
[17] Mittleman M H 1987 *Phys. Rev.* A **35** 4624–8
[18] Milstein A I, Müller C, Hatsagortsyan K Z, Jentschura U D and Keitel C H 2006 *Phys. Rev.* A **73** 062106
[19] Kuchiev M Yu and Robinson D J 2007 *Phys. Rev.* A **76** 012107
[20] Kuchiev M Yu 2007 *Phys. Rev. Lett.* **99** 130404
[21] Müller C, Voitkiv A B and Grün N 2003 *Nucl. Instrum. Methods Phys. Res.* B **205** 306–9
[22] Müller C, Voitkiv A B and Grün N 2003 *Phys. Rev.* A **67** 063407
[23] Müller C, Voitkiv A B and Grün N 2003 *Phys. Rev. Lett.* **91** 223601
[24] Müller C, Voitkiv A B and Grün N 2004 *Phys. Rev.* A **70** 023412
[25] Kamiński J Z, Krajewska K and Ehlotzky F 2006 *Phys. Rev.* A **74** 033402
[26] Sieczka P, Krajewska K, Kamiński J Z, Panek P and Ehlotzky F 2006 *Phys. Rev.* A **73** 053409
[27] Müller C, Deneke C and Keitel C H 2008 *Phys. Rev. Lett.* **101** 060402
[28] Müller C, Hatsagortsyan K Z and Keitel C H 2006 *Phys. Rev.* D **74** 074017
[29] Müller C, Hatsagortsyan K Z and Keitel C H 2008 *Phys. Lett.* B **659** 209–13
[30] Müller C, Hatsagortsyan K Z and Keitel C H 2008 *Phys. Rev.* A **78** 033408
[31] Schützhold R, Gies H and Dunne G 2008 *Phys. Rev. Lett.* **101** 130404
[32] Brodin G, Marklund M and Stenflo L 2001 *Phys. Rev. Lett.* **87** 171801
[33] Lundström E, Brodin G, Lundin J, Marklund M, Bingham R, Collier J, Mendonça J T and Norreys P 2006 *Phys. Rev. Lett.* **96** 083602
[34] Di Piazza A, Hatsagortsyan K Z and Keitel C H 2006 *Phys. Rev. Lett.* **97** 083603
[35] Heinzl T, Liesfeld B, Amthor K U, Schwoerer H, Sauerbrey R and Wipf A 2006 *Opt. Commun.* **267** 318–21
[36] Di Piazza A, Milstein A I and Keitel C H 2007 *Phys. Rev.* A **76** 032103
[37] Di Piazza A, Hatsagortsyan K Z and Keitel C H 2008 *Phys. Rev. Lett.* **100** 010403
[38] Lötstedt E, Jentschura U D and Keitel C H 2008 *Phys. Rev. Lett.* **101** 203001

[39] Roshchupkin S P 1983 *Izv. Vyssh. Uchebn. Zaved. Fiz.* **26** 12–5
Roshchupkin S P 1983 *Rus. Phys. J.* **26** 683 (Engl. Transl.)
[40] Borisov A V, Goryaga O G and Zhukovskii V C 1977 *Izv. Vyssh. Uchebn. Zaved. Fiz.* **20** 15–20
Borisov A V, Goryaga O G and Zhukovskii V C 1977 *Rus. Phys. J.* **20** 569 (Engl. Transl.)
[41] Borisov A V, Zhukovskii V C, Nasirov A K and Éminov P A 1981 *Izv. Vyssh. Uchebn. Zaved. Fiz.* **24** 12–5
Borisov A V, Zhukovskii V C, Nasirov A K and Éminov P A 1981 *Rus. Phys. J.* **24** 107 (Engl. Transl.)
[42] Roshchupkin S P 1985 *Yad. Fiz.* **41** 1244–57
Roshchupkin S P 1985 *Sov. J. Nucl. Phys.* **41** 796 (Engl. Transl.)
[43] Lötstedt E, Jentschura U D and Keitel C H 2007 *Phys. Rev. Lett.* **98** 043002
[44] Schnez S, Lötstedt E, Jentschura U D and Keitel C H 2007 *Phys. Rev.* A **75** 053412
[45] Bethe H A and Heitler W 1934 *Proc. R. Soc. Lond.* A **146** 83–112
[46] Becker W, Moore G T, Schlicher R R and Scully M O 1983 *Phys. Lett.* A **94** 131–4
[47] Volkov D M 1935 *Z. Phys.* **94** 250–60
[48] Leubner C 1981 *Phys. Rev.* A **23** 2877–90
[49] Dattoli G, Giannessi L, Mezi L and Torre A 1990 *Nuovo Cimento* B **105** 327–48
[50] Dattoli G, Torre A, Lorenzutta S, Maino G and Chiccoli C 1991 *Nuovo Cimento* B **106** 21–51
[51] Korsch H J, Klumpp A and Witthaut D 2006 *J. Phys. A: Math. Gen.* **39** 14947–64
[52] Reiss H R and Eberly J H 1966 *Phys. Rev.* **151** 1058–66
[53] Mitter H 1975 *Acta Phys. Austriaca Suppl.* **14** 397–468
[54] Ritus V I 1979 *Tr. Ordena Lenina Fiz. Inst. P N Lebedeva Akad. Nauk SSSR* **11** 5–151
Ritus V I 1985 *J. Rus. Laser Res.* **6** 497 (Engl. Transl.)
[55] Greiner W and Reinhardt J 1995 *Quantenelektrodynamik (Band VII der Lehrbuchreihe über Theoretische Physik)* 2nd edn (Frankfurt: Deutsch)
[56] Ringwald A 2001 *Phys. Lett.* B **510** 107–16
[57] Oleĭnik V P 1967 *Zh. Éksp. Teor. Fiz.* **52** 1049–67
Oleĭnik V P 1967 *Sov. Phys.—JETP* **25** 697 (Engl. Transl.)
[58] Bös J, Brock W, Mitter H and Schott T 1979 *J. Phys. A: Math. Gen.* **12** 715–31
[59] Panek P, Kamiński J Z and Ehlotzky F 2004 *Phys. Rev.* A **69** 013404
[60] Roshchupkin S P 2001 *Laser Phys.* **12** 498–503
[61] Becker W and Mitter H 1976 *J. Phys. A: Math. Gen.* **9** 2171–84
[62] Sarachik E S and Schappert G T 1970 *Phys. Rev.* D **1** 2738–53
[63] Reiss H R 1980 *Phys. Rev.* A **22** 1786–813